

NJC

Accepted Manuscript



This is an *Accepted Manuscript*, which has been through the Royal Society of Chemistry peer review process and has been accepted for publication.

Accepted Manuscripts are published online shortly after acceptance, before technical editing, formatting and proof reading. Using this free service, authors can make their results available to the community, in citable form, before we publish the edited article. We will replace this *Accepted Manuscript* with the edited and formatted *Advance Article* as soon as it is available.

You can find more information about *Accepted Manuscripts* in the [Information for Authors](#).

Please note that technical editing may introduce minor changes to the text and/or graphics, which may alter content. The journal's standard [Terms & Conditions](#) and the [Ethical guidelines](#) still apply. In no event shall the Royal Society of Chemistry be held responsible for any errors or omissions in this *Accepted Manuscript* or any consequences arising from the use of any information it contains.

**Polyacrylamide Modified Mesoporous SBA-16 Hybrids Encapsulated
with Lanthanide (Eu³⁺/Tb³⁺) Complex**

Ying Li,^{*a} Ruidan Zhu,^{a,b} Jie-Lin Wang,^{a,b} Xia Wang,^{*a} Shuang-He Liu^a

^a *School of Material Science and Engineering, University of Shanghai for Science and Technology, Shanghai 200093, P. R. China*

^b *School of Environment and Architecture, University of Shanghai for Science and Technology, Shanghai 200093, P. R. China*

* To whom the correspondence should be addressed. E-mail: liying@usst.edu.cn

Fax: +86-21-55270632. Phone: +86-21-55274069.

ABSTRACT

Novel luminescent polymer-functionalized mesoporous SBA-16 type hybrid materials with encapsulation of lanthanide (Eu^{3+} , Tb^{3+}) complexes for luminescence have been synthesized in situ. The organic molecule acrylamide (AM) was firstly modified by silane coupling agent 3-(triethoxysilyl)propylisocyanate (TEPIC) here to form the alkene precursor which thus be covalently bonded to mesoporous SBA-16 backbone through the co-hydrolysis and co-condensation reaction. Then the flexible polymer chain polyacrylamide (PAM) within the pores of SBA-16 can be formed by initiating the monomer. Through introducing the lanthanide ions and the typical ligand 1,10-Phenanthroline (phen), the luminescent mesoporous hybrids (denoted as $\text{Ln}(\text{S16-PAM-Si})_3$ and $\text{Ln}(\text{S16-PAM-Si})_3\text{phen}$, respectively) with the organic polymer acting as a flexible linker between the mesoporous framework and the lanthanide complex were finally attained. The results reveal that these materials exhibit high surface area, uniform mesostructure, efficient intramolecular energy transfer. Moreover, the ternary hybrids presents higher red/orange ratio, stronger luminescent intensity, longer lifetime and higher $^5\text{D}_0$ luminescence quantum efficiency than the binary one, suggesting the luminescent properties have been significantly improved with the introduction of the organic ligand phen.

Key words: luminescence, mesoporous SBA-16, polyacrylamide, $\text{Eu}^{3+}/\text{Tb}^{3+}$

1. Introduction

During the past decades, quite some research efforts have been dedicated to the areas of luminescent applications containing trivalent rare earth ions (e.g. fiber optic communication [1], OLEDs [2], and optical amplifiers [3]). Lanthanide emission covers spectra ranging from UV (Ce^{III} and Gd^{III}) to visible (Tm^{III} , Tb^{III} , Dy^{III} , Eu^{III} , and Sm^{III}) and further to near-infrared (Yb^{III} , Nd^{III} , Ho^{III} , and Er^{III}) regions, which makes lanthanides have great potential for the development of molecular electronics or biomedical analysis (e.g. bioprobes) [4-7]. However, due to the forbidden character of their intra-4f transitions, the trivalent lanthanide ions have very low molar absorption coefficients, which results in the limitation of practical application. Fortunately, this problem has been solved by selecting organic ligands to achieve the effective emission of the lanthanide ion through “antenna effect”. Considerable studies have been focused on the design and assembly of lanthanide complexes with organic ligands such as aromatic carboxylic acids, β -diketones and heterocyclic derivatives, which show strong absorption of ultraviolet light and then facilitate an effective intramolecular energy-transfer process to the central lanthanide ions [8-12].

For the application in optical devices, it is advantageous to incorporate lanthanide complexes in an inert host matrix such as silica-based materials [13-15], polymers [16, 17], and liquid crystal [18] to obtain the inorganic-organic hybrids.

Recently, the luminescence properties of lanthanide complexes supported on the solid matrix were studied extensively since their photophysical properties could be modified by interaction with the host structure. Much previous work has been done on physical mixing methods. However, these hybrid materials have many disadvantages such as the doping concentration of a complex silica matrix is very low and it is hard to obtain transparent and uniform material. Poor mechanical properties also restrict its practical application. Therefore, attention has been paid to grafting the ligands covalently to the silica backbone via Si-C bonds in which rare earth complexes luminescent centers are bonded with a siloxane matrix through Si-O linkage using different modified routes [19-21].

Ordered mesoporous silica materials are attractive hosts for the preparation and investigation of inorganic-organic hybrid materials, presenting a successive ordering from the molecular up to the macroscopic scale. Among them, SBA-15 appears much more attractive than other mesoporous silica because of its much larger unified pore size (up to 30 nm), thicker silica wall, and better stability. So it is easy to insert all kinds of lanthanide complexes into SBA-15, even large amounts of bulky molecules could be put into it. The research on linking the ternary lanthanide complexes to the mesoporous materials has shown promising visible-luminescence properties. While few researches on three-dimensional cubic structure of SBA-16 because of its hard

synthetic, but the material has high surface area, large cage and high thermal stability, especially for its three-dimensional pore connectivity obtains better mass transfer kinetics property than other one-dimensional pore system of hexagon. It also could be used as a good host material. Therefore, some research efforts, which have focused on preparing the organic/inorganic hybrids through functionalization of the exterior and/or interior surfaces, have promoted the utilization of mesoporous SBA-16 in many areas. To the best of our knowledge, the luminescence of lanthanide complex supported on the functionalized SBA-16 has been rarely reported to date. Recently, Yan group has done several studies on the synthesis and photoluminescence properties studies of lanthanide complexes covalently bonded to mesoporous SBA-16[22-24]. All these studies have shown that the promising visible-luminescent properties can be obtained by linking the lanthanide complexes to the mesoporous materials.

However, most of the mentioned hybrid material connected by covalent bonds merely contains the small organic ligand and the inorganic Si-O network, not the polymer within the organic chemistry region. So there exist some disadvantages for their application to the optical devices due to the restriction of their thermal stability and mechanical properties. And recently, more professional investigations have been altered to focus on the lanthanide hybrid materials concerning inorganic and organic polymerization reactions or imbedding certain polymers that contain long-carbon

chains by covalent bonds. It has been proved that the hybrid materials with the inorganic networks and organic polymers with high molecular weight have many excellent properties such as strong luminescence and high stability [24]. However, the synthesis and luminescence properties of lanthanide complexes covalently bonded with SBA-16 mesoporous materials in situ by the modified polymer have not been explored to date.

Based on the discussion above, covalent grafting of lanthanide complexes to the polymer functionalized mesoporous and the subsequent study on such hybrid material is of fundamental importance, and therefore draws considerable research interest. In this paper, we insert an organic polymer polyacrylamide as a flexible linker between the lanthanide complex and the mesoporous silica framework. A novel method has been presented to connect lanthanide complexes to the modified mesoporous SBA-16 by polyacrylamide (PAM), resulted in obtaining the polymeric mesoporous hybrid material with high luminescent and thermal stabilities. The detailed characterization of the polymer functionalized mesoporous hybrid is investigated and especially the photoluminescent properties of binary and ternary hybrids are compared in our study.

2. Experimental section

2.1 Materials

Pluronic F127 (EO₁₀₆PO₇₀EO₁₀₆, Lancaster), tetraethoxysilane (TEOS, Aldrich),

and 3-(triethoxysilyl)-propyl-isocyanate (TEPIC, Lancasater) are all analytically pure reagents, the solvents are ethanol and tetrahydrofuran (THF). 1,10-phenanthroline (Phen), acrylamide (AM), benzoyl peroxide (BPO) were purchased from Sinopharm Chemical Reagent Co., Ltd. Other reagents were used as received. $\text{Ln}(\text{NO}_3)_3$ ($\text{Ln} = \text{Eu}, \text{Tb}$) was prepared by dissolving their corresponding oxides in excess concentrated nitric acid (HNO_3).

2.2 Synthetic procedures

2.2.1 Synthesis of micromolecule precursor AM-Si

Acrylamide (AM) was first dissolved in a suitable volume of anhydrous THF, and TEPIC was added with a molar ratio of 1:1, then the mixture was refluxed at 70 °C for 12 h under stirring in a nitrogen atmosphere. Next, the solvent was distilled off under reduced pressure, yielding the alkoxy silane modified acrylamide AM-Si: a deep orange oil-like liquid. AM-Si ($\text{C}_{13}\text{H}_{26}\text{O}_5\text{SiN}_2$) ^1H NMR data: δ 6.0 (H, bs, NH), δ 5.02 (H, m, $\text{CH}_2=$), δ 5.16 (H, m, $\text{CH}_2=$), δ 4.45 (H, t, =CH), δ 1.11 (9H, m, $\text{CH}_3(\text{OEt})$), δ 3.2 (2H, dt, $\text{N}(\text{CH}_2)_3$), δ 3.33 (2H, t, $\text{N}(\text{CH}_2)_3$), δ 3.63 (2H, t, $\text{N}(\text{CH}_2)_3$), δ 3.57 (6H, dt, $\text{CH}_2(\text{OEt})$) ; elemental analysis calcd(%) for $\text{C}_{13}\text{H}_{25}\text{O}_5\text{N}_2\text{Si}$ (317.44): C 49.18 ,H 7.94 ,Si 8.85, N 8.83,O 25.20;found: C 48.46 ,H 8.05 ,Si 8.62, N 8.78,O 25.48

2.2.2 Synthesis of PAM-functionalized SBA-16 mesoporous material (Denoted as S16-PAM-Si)

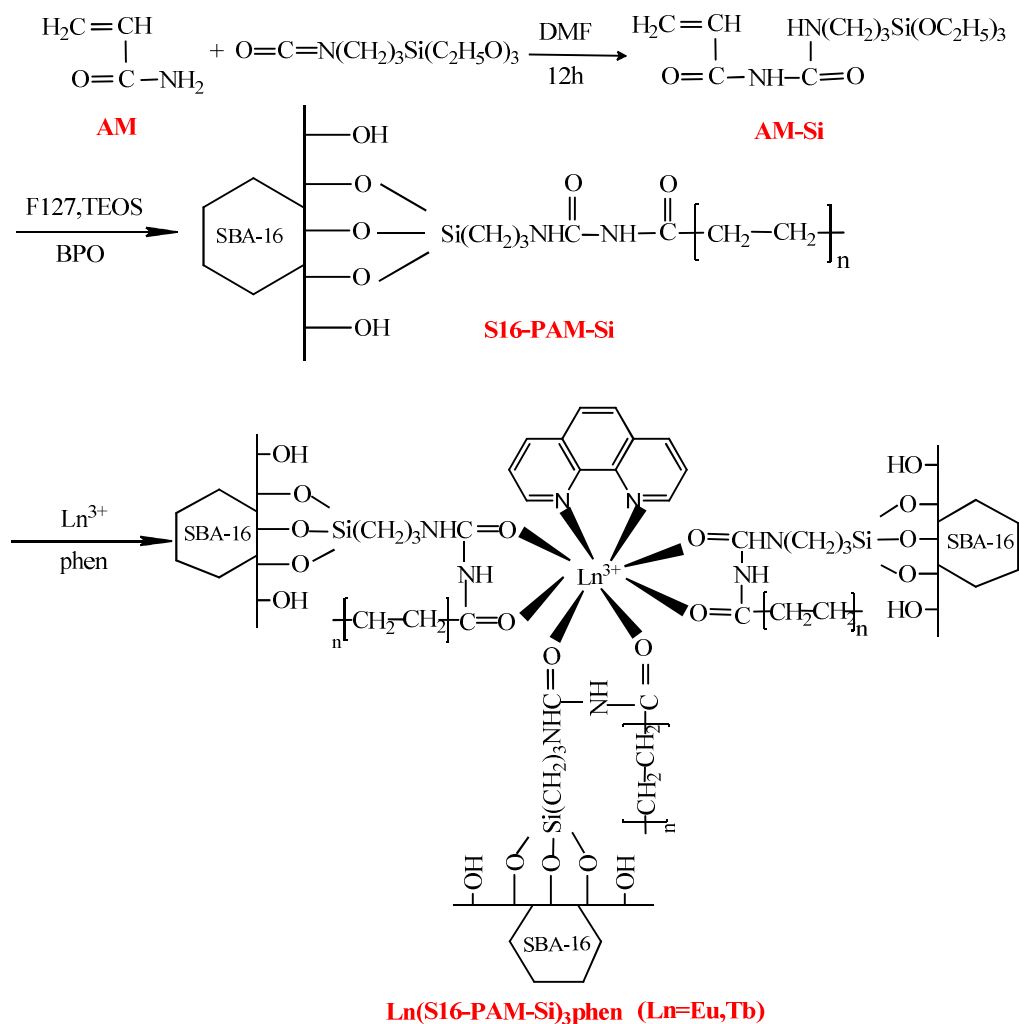
PAM-functionalized SBA-16 mesoporous material (S16-PAM-Si) was synthesized from acidic mixture with the following molar composition F127 : TEOS : AM-Si : HCl : H₂O = 0.0040 : 0.96 : 0.04 : 4 : 130. F127 (0.508 g) was dissolved in deionized water (3.4 g) and 2 mol/L HCl solution (20 g) at 35 °C. A mixture of AM-Si and TEOS was added into the above solution at 35 °C with stirring for 24 h and transferred into a Teflon bottle sealed in an autoclave, which was heated at 100 °C for 48 h. Then the solid product was filtrated, washed thoroughly with deionized water and air-dried for 12 h at 60 °C. Removal of copolymer surfactant F127 was conducted by Soxhlet extraction with ethanol under reflux for 2 days to give the sample denoted as S16-AM-Si. Then the S16-AM-Si (1mmol) was dissolved in 20 ml N,N-dimethylformamide (DMF) with stirring and 1% quality of the momomer initiator Benzoyl peroxide (BPO) was added. The mixture was refluxed at 50 °C for 4 h in the nitrogen atmosphere. After isolation, the brown black viscous liquid product S16-PAM-Si was obtained.

2.2.3 Synthesis of PAM-functionalized SBA-16 mesoporous material Covalently Bonded with the Binary Ln³⁺ Complexes (Denoted as Ln(S16-PAM-Si)₃, Ln=Eu, Tb)

S16-PAM-Si was added in an appropriate amount of Ln(NO₃)₃ ethanol solution with the molar ratio of Ln³⁺ : S16-PAM-Si= 1 : 3. After refluxing at 75 °C for 12 h, the mixture was dried at 65 °C in a vacuum.

2.2.4 Synthesis of PAM-functionalized SBA-16 mesoporous material Covalently Bonded with the Ternary Ln^{3+} Complexes (Denoted as $\text{Ln}(\text{S16-PAM-Si})_3\text{phen}$, $\text{Ln}=\text{Eu}, \text{Tb}$)

The synthesis procedure for $\text{Ln}(\text{S16-PAM-Si})_3\text{phen}$ was similar to that of $\text{Ln}(\text{S16-PAM-Si})_3$ except that the molar ratio was replaced by $\text{Ln}^{3+} : \text{S16-PAM-Si} : \text{phen} = 1 : 3 : 1$. The predicted structure of $\text{Ln}(\text{S16-PAM-Si})_3\text{phen}$ was outlined in Scheme 1.



Scheme 1. Synthesis procedure and predicted structure of ternary hybrid mesoporous material $\text{Ln}(\text{S16-PAM-Si})_3\text{phen}$.

2.3 Physical Measurement

^1H NMR spectrum was recorded in CDCl_3 on a Bruker AVANCE-400 spectrometer with tetramethylsilane (TMS) as an internal reference. Elemental FTIR spectra were recorded using a Perkin Elmer Spectrum 100 FTIR spectrophotometer with the KBr pellet technique within the $4000\text{--}400\text{ cm}^{-1}$ region. The Ultraviolet absorption spectra were carried out on an Agilent 8453 spectrophotometer. X-ray powder diffraction (XRD) patterns were recorded on a Rigaku D/max-rB diffractometer equipped with graphite monochromatized $\text{Cu K}\alpha$ radiation ($\lambda=0.15405\text{ nm}$) in a 2θ range from 0° to 5° . Nitrogen adsorption/desorption isotherms were collected at liquid nitrogen temperature on a Nova 1000 analyzer. Surface areas were recorded by the Brunauer-Emmett-Teller (BET) method, pore size distributions were carried out by the desorption branches of the nitrogen isotherms from the Barrett-Joyner-Halenda (BJH) model. The fluorescence excitation and emission spectra were obtained on a RF-5301 spectrophotometer (wavelength resolution was 0.5 nm), equipped with a stable spec-xenon lamp as the light source. And the fluorescence decay properties were carried out on an Edinburgh FLS920 phosphorimeter. Transmission electron microscope (TEM) experiments were conducted on a JEOL2011 microscope operated at 200 kv or on a JEM-4000EX microscope operated at 400 kv . Thermogravimetry analysis (TGA) was performed on a Pyris 1 TGA at a heating rate

of 15 °C/min, 3~8 mg of powder under nitrogen atmosphere.

3. Results and Discussion

3.1 The Formation Process of Polyacrylamide Modified Mesoporous SBA-16 Hybrids

A kind of novel polymer-functionalized mesoporous materials $\text{Ln}(\text{S16-PAM-Si})_3$ and $\text{Ln}(\text{S16-PAM-Si})_3\text{phen}$ were synthesized in situ, and the predicted structure of hybrids are shown in Scheme.1. Generally it is very difficult to prove the exact structure of this kind of non-crystalline hybrid materials and it is hardly possible to solve the coordination behavior of lanthanide ions. However, according to the rare-earth coordination chemistry principle and the organic functional groups, the main composition and coordination effect can be predicted. The lanthanide positive ions are hard Lewis acids, so they readily coordinate with hard bases containing oxygen atom and nitrogen atom. In addition, it is most stable for the lanthanide complex to exist with the coordination number of 8 or 9. Therefore, we prepared the material by adding the appropriate and accurate proportion of reagent into the system in our experiment ($\text{S16-PAM-Si} : \text{Ln}^{3+} : \text{phen} = 3:1:1$) to obtain the hybrids materials of relatively stable structure. On the other hand, the selection of the polymer ligand is the key point for the preparation of this hybrid material. Herein, the Polyacrylamide ligand PAM is selected as a multifunctional linker, which not only can be covalently bonded to the framework of mesoporous silica SBA-16 through the method of

modified amino group, but also can coordinate to the Ln^{3+} ion as well as sensitive the luminescence properties.

3.2 The precursor AM-Si and PAM-functionalized SBA-16 mesoporous material

The FTIR spectra of AM (A), AM-Si (B) and PAM-functionalized mesoporous material S16-PAM-Si (C) are compared to prove successful preparation of the precursor and hybrids, whose main absorptions and assignments are presented in Fig.

1. Compared with the free ligand AM (Fig. 1A), it can be observed that the AM-Si (Fig. 1B) spectra appears a strong broadband located at 2977, 2927 and 2885 cm^{-1} which originates from the three methylene groups of TEPIC. In addition, the spectra of AM-Si are dominated by stretching vibration absorption bands ν (Si-C, 1165 cm^{-1}) and ν (Si-O, 1078 cm^{-1}) which proved the fact that the hydrolysis of AM-Si precursor has not occurred, and moreover, ^1H NMR spectra relative to the precursors are in full agreement with the proposed structures (Scheme 1). Furthermore, the band centered at 3336 cm^{-1} was attributed to the stretching vibration of grafted $-\text{NH}$ group. The bending vibration (δ_{NH} , 1530 cm^{-1}) further proved that TEPIC was successfully grafted onto AM ligand. The spectra of mesoporous hybrid material (Fig. 1C) indicated the formation of a Si-O-Si framework, which is evidenced by the broad bands located at 1078 cm^{-1} (ν_{as} , Si-O), 800 cm^{-1} (ν_{s} , Si-O) [19] (ν_{as} -asymmetric stretching vibration, ν_{s} -symmetric stretching vibration). Furthermore, the bands at 1660 cm^{-1} originating from $-\text{CONH}-$ group of AM-Si can also be observed in panel C

of Fig. 1, which is consistent with the fact that the PAM group in the framework remains intact after both hydrolysis-condensation reaction and the surfactant extraction procedure [25].

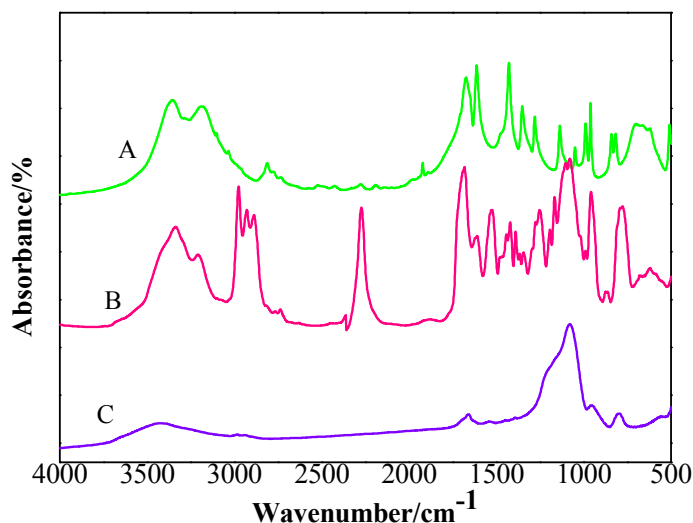


Fig. 1 FTIR spectra of the free ligand AM (A), the precursor AM-Si (B), and the mesoporous hybrid material S16-PAM-Si (C).

The ultraviolet absorption spectra of AM (A) and AM-Si (B) are presented in Fig. 2. From the spectra, it can be observed that an obvious blue shift (about 4 nm) of the major π - π^* electronic transitions (A \rightarrow B: from 234 to 230 nm), which indicates the electron distribution of the modified AM-Si has been changed in comparison with the free ligand AM as a result of the TEPIC graft. It can be inferred that the difference between the energy levels of the electron transitions of the new electronic conjugating system was enlarged after the modification of AM.

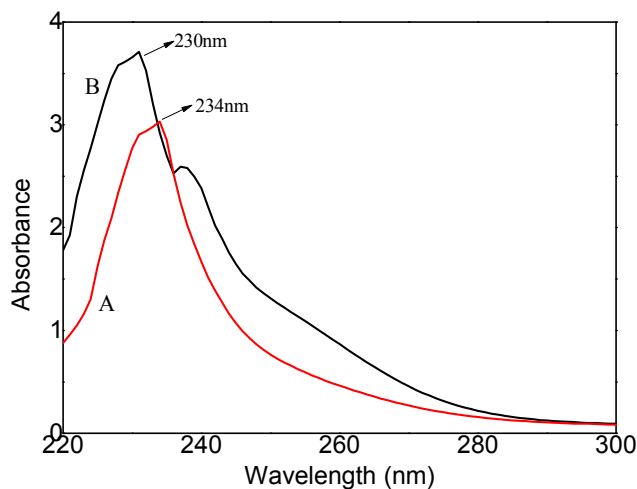


Fig. 2 The ultraviolet absorption spectra of AM (A) and AM-Si (B).

3.3 The structure of PAM-functionalized SBA-16 mesoporous material covalently Bonded with the binary and Ternary Ln^{3+} Complexes

The small-angle X-ray diffraction (SAXRD) patterns and nitrogen adsorption/desorption isotherms are popular and efficient methods to characterize highly ordered mesoporous material. The powder SAXRD patterns of SBA-16(A) and Tb(S16-PAM-Si)₃(B), Eu(S16-PAM-Si)₃(C), Tb(S16-PAM-Si)₃phen(D), Eu(S16-PAM-Si)₃phen (E) are depicted in Fig. 3. All of the materials exhibit the typical X-ray diffraction patterns of the 2D hexagonal pore ordering of the P6mm space group. As shown in Fig. 3, for the binary and ternary materials, they all display well-resolved patterns with a prominent peak accompanied by two weak peaks, indexed as (110), (200), and (211) reflections corresponding to P6mm hexagonal symmetry, respectively, which matches well with the pattern of the SBA-16 (Fig.3a). Compared with the pure SBA-16 (see Table 1), the d_{100} spacing values of the four materials are

nearly unchanged, respectively, indicating that their framework hexagonal ordering has been preserved well after the introduction of the $\text{Ln}(\text{PAM})_3$ components. It is also worth noting that the binary and ternary materials exhibit decreased diffraction intensity as compared with the SBA-16 material. This is probably due to the presence of $\text{Ln}(\text{PAM})_3$ inside the pore channels of the hybrid materials $\text{Ln}(\text{S16-PAM-Si})_3$ and $\text{Ln}(\text{S16-PAM-Si})_3\text{phen}$, respectively.

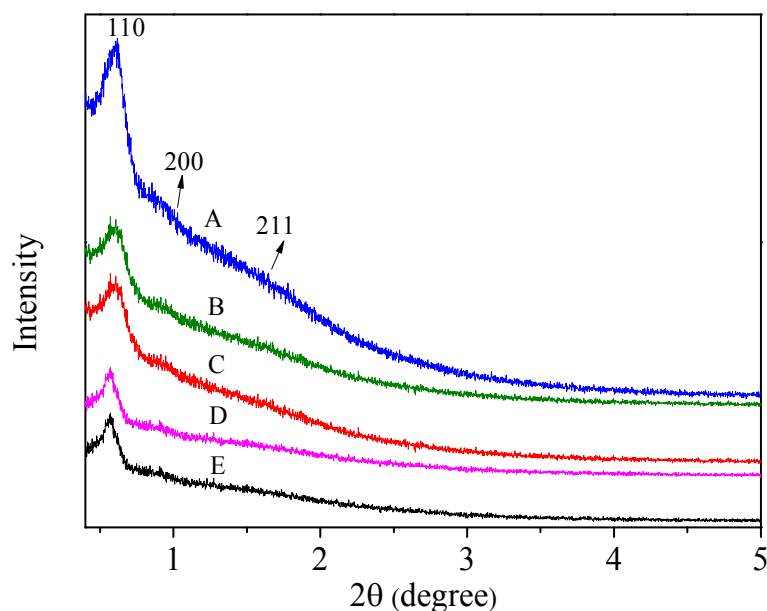


Fig. 3 SAXRD patterns of SBA-16(A), $\text{Tb}(\text{S16-PAM-Si})_3$ (B), $\text{Eu}(\text{S16-PAM-Si})_3$ (C), $\text{Tb}(\text{S16-PAM-Si})_3\text{phen}$ (D), $\text{Eu}(\text{S16-PAM-Si})_3\text{phen}$ (E)

Fig. 4 displays the N_2 adsorption-desorption isotherms of SBA-16, $\text{Tb}(\text{S16-PAM-Si})_3$, $\text{Tb}(\text{S16-PAM-Si})_3\text{phen}$, $\text{Eu}(\text{S16-PAM-Si})_3$ and $\text{Eu}(\text{S16-PAM-Si})_3\text{phen}$ materials, respectively. They all show typical type IV isotherms with an H1 type hysteresis loop similar to that of the SBA-16 material, characteristic of mesoporous materials

according to the IUPAC classification [26]. The structure data of all of these mesoporous materials (BET surface area, total pore volume, and pore size, etc.) are summarized in Table 1. It can be observed that the surface area, pore volume, and pore size of the $\text{Ln}(\text{S16-PAM-Si})_3$ ($\text{Ln}=\text{Eu}, \text{Tb}$) and $\text{Ln}(\text{S16-PAM-Si})_3\text{phen}$ ($\text{Ln}=\text{Eu}, \text{Tb}$), as expected, decrease after introducing the $\text{Ln}(\text{PAM})_3$ ($\text{Ln}=\text{Eu}, \text{Tb}$) complexes into the SBA-16 material. This phenomenon originates from the dispersion of the lanthanide complexes on the surface of the SBA-16 material since these complexes that dispersed inside the channel would enhance the roughness of the pore surfaces and then make the surface area, pore volume, and pore size of these materials much smaller than those of the pure SBA-16 [22].

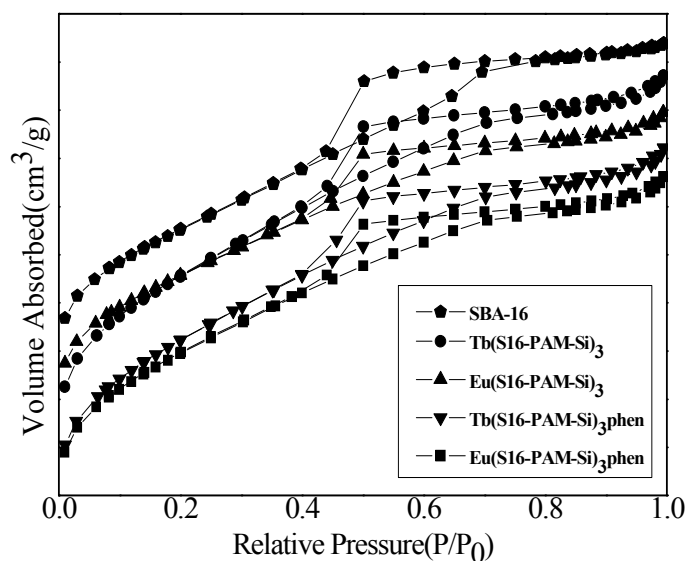


Fig. 4 N_2 adsorption/desorption isotherms of pure SBA-16 and mesoporous hybrids.

Meanwhile, the three-dimensional cubic pore structure of $\text{Ln}(\text{S16-PAM-Si})_3\text{phen}$ is further confirmed by a TEM micrograph (see Fig. 5). As shown in the Fig. 5, the PAM-functionalized mesoporous materials $\text{Eu}(\text{S16-PAM-Si})_3\text{phen}(\text{A})$ and $\text{Tb}(\text{S16-PAM-Si})_3\text{phen}(\text{B})$ all present a highly ordered three-dimensional cubic pore structure which is the characteristic of mesoporous SBA-16 material. It confirms that the suggested $p6mm$ symmetry and a well-ordered hexagonal structure, which is also in agreement with the SAXRD and N_2 adsorption/desorption isotherms. The distance between the centers of the mesopore is estimated to be 16.12 nm, in good agreement with the value determined from the corresponding XRD data (see Table. 1).

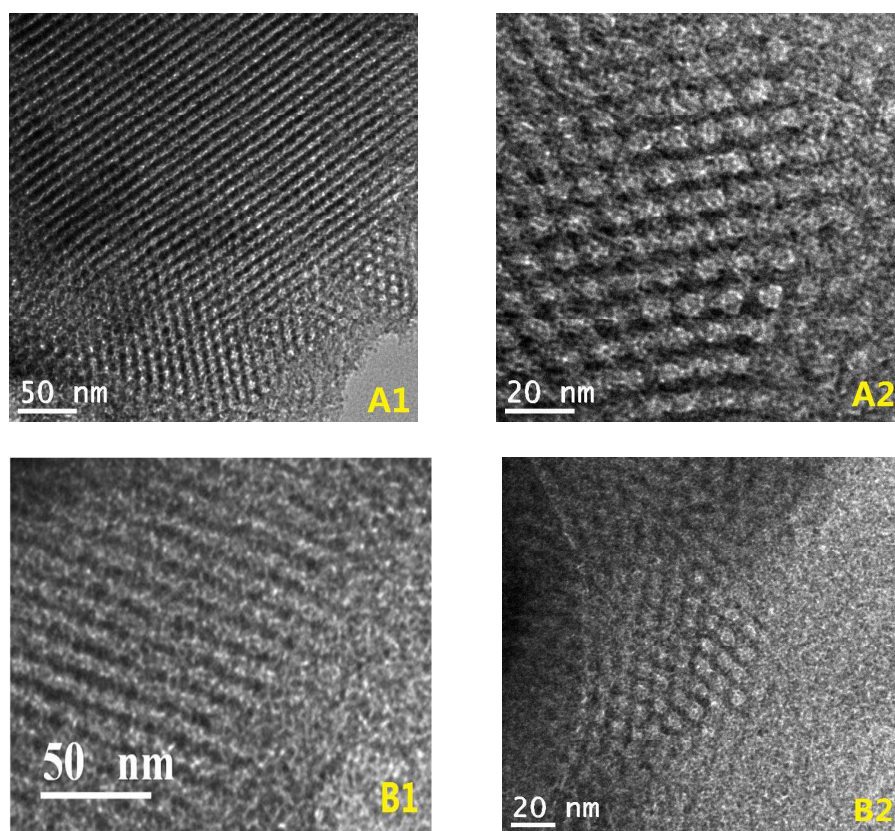


Fig. 5 HRTEM images of $\text{Eu}(\text{S16-PAM-Si})_3\text{phen}(\text{A})$ and $\text{Tb}(\text{S16-PAM-Si})_3\text{phen}(\text{B})$ recorded along the [100] (A1,B1) and [110] (A2,B2) zone axes.

Table 1 Textural Data of SBA-16, Tb(S16-PAM-Si)₃, Eu(S16-PAM-Si)₃, Tb(S16-PAM-Si)₃phen, Eu(S16-PAM-Si)₃phen

Sample	d ₁₀₀ (nm)	a ₀ (nm)	S _{BET} (m ² /g)	V(cm ³ /g)	D _{BH} (nm)	t(nm)
SBA-16	15.56	17.97	836	0.67	3.47	2.41
Tb(S16-PAM-Si) ₃	15.30	17.67	784	0.63	3.26	2.37
Eu(S16-PAM-Si) ₃	14.48	16.72	731	0.58	3.24	2.24
Tb(S16-PAM-Si) ₃ phen	14.30	16.51	659	0.54	3.22	2.21
Eu(S16-PAM-Si) ₃ phen	14.29	16.51	660	0.57	3.23	2.22

d₁₀₀ is the d(100) spacing, a₀ is the cell parameter ($a_0=2d_{100}/\sqrt{3}$), S_{BET} is the BET surface area, V is the pore volume, D is the pore diameter, and t is the wall thickness, calculated by a₀-D.

3.3 The properties of PAM-functionalized SBA-16 mesoporous material covalently Bonded with the binary and Ternary Ln³⁺ Complexes

Fig. 6 shows the thermogravimetry trace (TGA) (a) and differential thermogravimetry trace (DTG) (b) of the hybrid mesoporous material Eu(S16-PAM-Si)₃phen. From the TGA curve (Fig. 6a), we can observe that the sample shows three main steps in weight loss, the first step of the hybrid material Eu(S16-PAM-Si)₃phen weight loss has lost mass about 5.0% from 50 to 200 °C. It is deduced that the adsorbed water and residual solvent evaporated, without any decomposition of the chemical bonds. The second step of weight loss is about 10% between 200 and 450 °C corresponding to the decomposition of the polymer PAM since PAM occupies about 10% of the molecular weight. In addition, the hybrid material has lost weight with the most rapid speed when the temperature has climbed to 377 °C, which is observed from the DTG data with the sharpest peak at 377 °C. The last step of weight loss is about 5% from 450 to 700°C which is attributed to the first decomposition of organic ingredient phen. From the TGA curve of the hybrid system, it can be concluded that

the introduction of mesoporous and polymer can improve the thermal stability compared to the general europium complexes, whose thermal decomposition often occur at around 200-300 °C [27, 28].

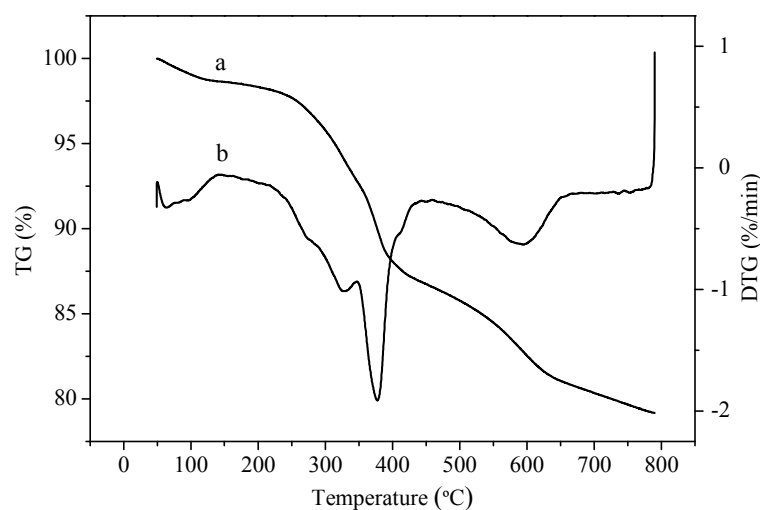


Fig. 6 Thermo gravimetric (TG) and Differential thermal gravity (DTG) curves of Eu(S16-PAM-Si)₃phen .

Fig. 7 presents the excitation (A) and emission (B) spectra of the binary hybrid Eu(S16-PAM-Si)₃ and the ternary hybrid Eu(S16-PAM-Si)₃phen. The excitation spectra (Fig. 7A) of the two europium hybrid mesoporous materials were monitored at 614 nm, which both exhibit a broad excitation band centered at 350 nm in the long-wavelength UV range, which can be ascribed to the charge transfer state (CTS) of Eu-O [29], and no apparent excitation of phen is observed. The strong CTS absorption is favorable for the efficient energy migration of Eu³⁺, and the effective luminescence of Eu³⁺ can be expected. Besides, weak absorption bands in the range of the short

wavelength ultraviolet region of 200-300 nm occur, corresponding to the host absorption of the Si-O network. No f-f transitions could be observed in the spectra (they are too weak).

The luminescence behaviors of the two europium hybrid mesoporous materials have been investigated at 298K by direct excitation of the ligands (350 nm). Representative emission spectra with narrow-width red emissions are given in Fig.7B, and the detailed luminescent data are shown in Table.2 The emission bands are assigned to the ${}^5D_0 \rightarrow {}^7F_0$, ${}^5D_0 \rightarrow {}^7F_1$, ${}^5D_0 \rightarrow {}^7F_2$, ${}^5D_0 \rightarrow {}^7F_3$, and ${}^5D_0 \rightarrow {}^7F_4$ transitions at approximately 592, 596, 614, 649 and 662 nm, respectively. For the emission spectrum, the predominant transition is ${}^5D_0 \rightarrow {}^7F_2$ at approximately 614 nm, corresponding to a typical electric dipole transition, and this transition strongly varies with the local symmetry of Eu^{3+} , whereas the ${}^5D_0 \rightarrow {}^7F_1$ transition corresponds to a parity-allowed magnetic dipole transition, which is independent of the host material. When the interactions of the rare-earth complex with its local chemical environment are stronger, the complex becomes more nonsymmetrical, and the intensity of the electric-dipolar transitions becomes more intense. As a result, the intensity (the integration of the luminescent band) ratio of the ${}^5D_0 \rightarrow {}^7F_2$ transition to the ${}^5D_0 \rightarrow {}^7F_1$ transition has been widely used as an indicator of Eu^{3+} site symmetry [30,31]. Therefore, the emission spectrum indicates that the Eu^{3+} site is situated in an

environment without inversion symmetry [32, 33]. The asymmetric microenvironment induces polarization of the Eu^{3+} because of the influence of the ligand's electric field on the electric dipole transition probability.

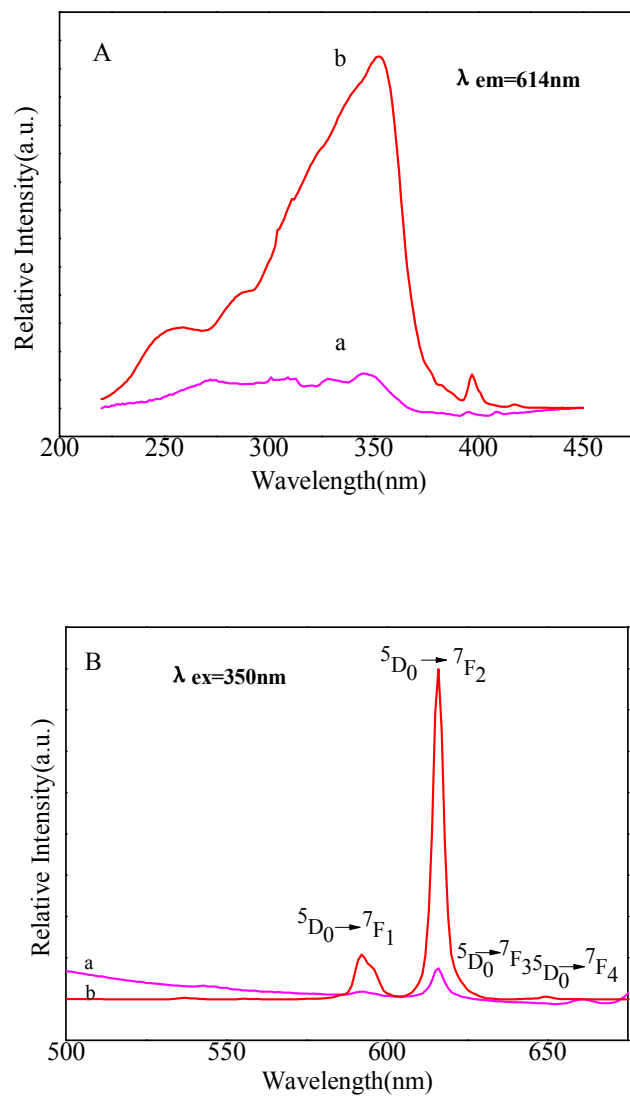


Fig. 7 The excitation (A) and emission (B) spectra of the europium mesoporous hybrid materials: $\text{Eu}(\text{S16-PAM-Si})_3$ (a) and $\text{Eu}(\text{S16-PAM-Si})_3\text{phen}$ (b).

Fig. 8 presents the excitation (A) and emission (B) spectra of $\text{Tb}(\text{S16-PAM-Si})_3$ and $\text{Tb}(\text{S16-PAM-Si})_3\text{phen}$ mesoporous hybrid materials. The similar excitation

spectra of the two hybrid materials were obtained by monitoring the corresponding emission wavelength of the Tb^{3+} ion at 545 nm. As shown in Fig. 8A, a broad excitation band extending from 220 to 450 nm are dominated by the peak centered at 354 nm, which can be assigned to the conjugating $\pi \rightarrow \pi^*$ electron transition of the ligand [34,35]. The emission bands (Fig. 8B) of the mesoporous hybrid materials were assigned to the ${}^5D_0 \rightarrow {}^7F_J$ ($J = 3-6$) transitions at 492, 545, 584, and 619 nm respectively, under excitation at wavelengths of 354 nm. As for the binary hybrid $Tb(S16-PAM-Si)_3$, we could observe only two bands at 492 and 545 nm originating from ${}^5D_0 \rightarrow {}^7F_6$ and ${}^5D_0 \rightarrow {}^7F_5$, respectively, while the bands originating from ${}^5D_0 \rightarrow {}^7F_4$ and ${}^5D_0 \rightarrow {}^7F_3$ transitions are so weak at 584 and 619 nm that they cannot be seen clearly from the emission spectra of the samples. This suggests that an inefficient energy transfer process occurred between PAM-Si and terbium ions. After the introduction of the organic ligand phen, the emission intensities of ternary hybrid $Tb(S16-PAM-Si)_3phen$ show significant luminescence enhancement, which indicates that the corporation effect of the polymer PAM and the second ligand phen could well sensitize luminescence of Tb^{3+} ion. In brief, the hybrids $Eu(S16-PAM-Si)_3phen$ and $Tb(S16-PAM-Si)_3phen$ showed the intense red and green photoluminescence respectively when irradiated with UV radiation (See Fig.9).

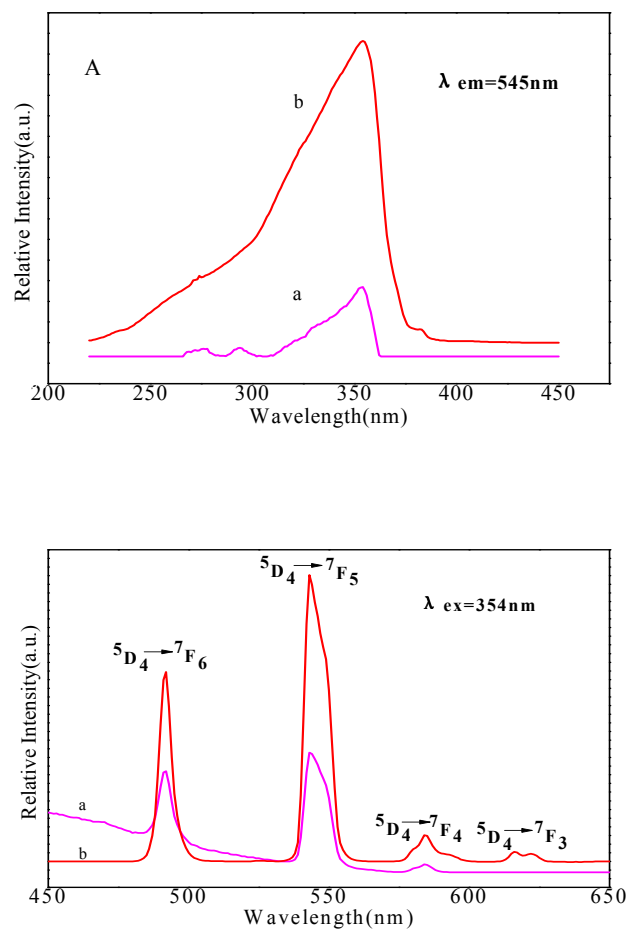


Fig. 8 The excitation (A) and emission (B) spectra of the terbium mesoporous hybrid materials: $\text{Tb}(\text{S16-PAM-Si})_3$ (a) and $\text{Tb}(\text{S16-PAM-Si})_3\text{phen}$ (b).



Fig. 9 Luminescence of $\text{Eu}(\text{S16-PAM-Si})_3\text{phen}$ (red) and $\text{Tb}(\text{S16-PAM-Si})_3\text{phen}$ (green) under ultraviolet irradiation.

The typical decay curves of the Eu^{3+} and Tb^{3+} hybrid mesoporous materials were measured, and they can be described as a single exponential $\ln[S(t)/S_0] = -k_1t = -t/\tau$, indicating that all Eu^{3+} and Tb^{3+} ions occupy the same average coordination environment. Furthermore, we selectively determined the emission quantum efficiencies (η) of the ${}^5\text{D}_0$ europium ion excited state for Eu^{3+} hybrids on the basis of the emission and the detailed luminescent data were shown in Table 2.

Table 2 Photo luminescent data of the mesoporous materials

	$\text{Eu}(\text{S16-PAM-Si})_3$	$\text{Eu}(\text{S16-PAM-Si})_3\text{phen}$
$\nu_{00}(\text{cm}^{-1})$	16892	16892
$\nu_{01}(\text{cm}^{-1})$	16778	16778
$\nu_{02}(\text{cm}^{-1})$	16287	16287
$\nu_{03}(\text{cm}^{-1})$	15408	15408
$\nu_{04}(\text{cm}^{-1})$	15106	15106
$I_{01}(\text{a.u.})$	19.39	110.83
$I_{02}(\text{a.u.})$	79.38	807.40
I_{02}/I_{01}	4.09	7.29
$\tau(\text{ms})$	0.611	0.960
$1/\tau(\text{ms}^{-1})$	1.64	1.04
A_r	321.08	475.29
A_{nr}	1318.92	564.71
$\eta(\%)$	19.58	45.70
$\Omega_2(\times 10^{-20} \text{cm}^2)$	6.11	10.88
$\Omega_4(\times 10^{-20} \text{cm}^2)$	0.98	0.25

Here, ν_{0j} represents the wavenumber of ${}^5\text{D}_0\text{-}{}^7\text{F}_j$ emission lines, I_{0j} represents detected intensity of ${}^5\text{D}_0\text{-}{}^7\text{F}_j$ emission, τ represents ${}^5\text{D}_0$ lifetime, A_r and A_{nr} represent radiative and nonradiative decay rates respectively, η represents luminescence quantum efficiency

As we can see from Table 2, $\text{Eu}(\text{S16-PAM-Si})_3\text{phen}$ ($\eta = 45.70\%$) exhibits a much higher emission quantum efficiency than $\text{Eu}(\text{S16-PAM-Si})_3$ ($\eta = 19.58\%$), which indicates that the introduction of the phen ligand can efficiently activate the luminescence of the Eu^{3+} ion.

Furtherly, we determined the Judd-Ofelt Parameters for the three covalently bonded europium hybrid materials. The spontaneous emission probability, A , of the

transition is related to its dipole strength according to eq 1. [36]

$$A = (64\pi^4\nu^3)/[3h(2J+1)]\{[(n^2+2)^2/9n]S_{(ED)} + n^2S_{(MD)}\} \quad (1)$$

ν is the average transition energy in cm^{-1} , h is Planck constant, $2J+1$ is the degeneracy of the initial state (1 for 5D_0). $S_{(ED)}$ and $S_{(MD)}$ are the electric and magnetic dipole strengths, respectively. The factors containing the medium's refractive index n result from local field corrections that convert the external electromagnetic field into an effective field at the location of the active center in the dielectric medium. Among all the transitions from 5D_0 to ${}^7F_{0,3,5}$ ($J = 0, 3, 5$) are forbidden both in magnetic and induced electric dipole schemes ($S_{(ED)}$ and $S_{(MD)}$ are zero). The transition from 5D_0 to 7F_1 ($J = 1$) is the isolated magnetic dipole transition and has no electric dipole contribution, which practically independent of the ion's chemical environment and can be used as a reference as above mentioned. Besides, the ${}^5D_0 \rightarrow {}^7F_6$ transition could not be experimentally detected and it is not necessary to determine its J-O parameter. So we only need to estimate the two parameters (Ω_2, Ω_4) related to the two purely induced electric dipole transitions ${}^5D_0 \rightarrow {}^7F_{2,4}$ on basis of only three parameters Ω_i using eq 2. [37]

$$A = (64e^2\pi^4\nu^3)/[3h(2J+1)]\{[(n^2+2)^2/9n]\sum\Omega_i|\langle J||U^{(\lambda)}||J'\rangle|^2 \quad (2)$$

e is the electronic charge. With the refraction index $n = 1.506$, [38] and $|\langle J||U^{(\lambda)}||J'\rangle|^2$ values are the square reduced matrix elements whose values are

0.0032 and 0.0023 for $J = 2$ and 4,[39] respectively. The Ω_2 , Ω_4 intensity parameters for the two hybrid materials are shown in Table 2. The distinction of the two intensity parameters for the two hybrids is not apparent, suggesting that the Eu^{3+} ion is located in a polarizable chemical environment for luminescence.

4. Conclusions

In summary, we have developed a representative method for preparing the novel polymeric mesoporous luminescent hybrids by linking the binary and ternary Eu^{3+} ion complexes to the functionalized mesoporous SBA-16 with the modified polyacrylamide by cocondensation of tetraethoxysilane in the presence of Pluronic F127 as a template. All the resulting materials preserve their mesoscopically ordered structures and show highly uniform pore size distributions. Further investigation into the luminescence properties of binary and ternary polymeric mesoporous hybrid materials show that the characteristic luminescence of the corresponding rare earth ions through intramolecular energy transfers from the modified ligand to the rare earth ions. In addition, the ternary polymeric hybrid materials exhibit stronger luminescent intensities, longer lifetimes, and higher quantum efficiencies than binary ones for the introduction of organic ligand phen. It is rather meaningful that Polyacrylamide could be initially introduced in SBA-16 through covalent bonds that may heavily affect the photostability or thermal stability of rare earth- Polyacrylamide complexes. The

excellent luminescent properties of these materials, together with the highly ordered hexagonal channel structures and uniform tunable pore sizes of the organic group functionalized SBA-15 mesoporous materials will expand their applications in optical or electronic areas.

Acknowledgments

This work was supported by the National Natural Science Foundation of China (21101107,51173107), the innovation Project of the Shanghai Municipal Education Commission (No.15ZZ076), the Hujiang Foundation of China (B14006).

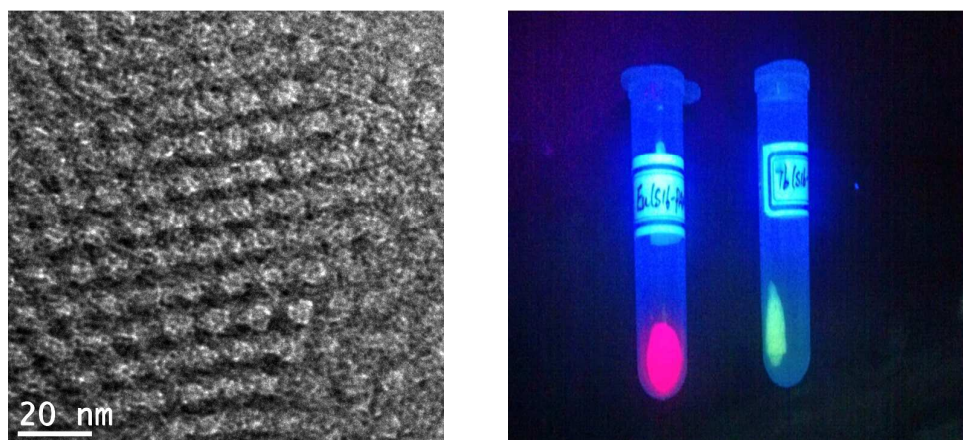
References

- [1] J.M. Lopez-Higuera, Handbook of Optical Fibre Sensing Technology, Wiley-VCH, Weinheim, Germany, 2002.
- [2] Y. Zhang, C. Li, H.H. Shi, B. Du, W. Yang, Y. Cao, New. J. Chem., 2007, **31** 569-574.
- [3] W.H. Wong, E.Y.B. Pun, K.S. Chan, Appl. Phys. Lett., 2004, **84**, 176-178.
- [4] K. Binnemans, Chem. Rev., 2009, **109**, 4283-4374.
- [5] L.D. Carlos, R.A.S. Ferreira, V.Z. Bermudez, S.J.L. Ribeiro, Adv. Mater., 2009, **21** 509-534.
- [6] J.-C.G. Bunzli, Chem. Rev., 2010, **110**, 2729-2755.
- [7] Y.Liu, L.N. Sun, J. L.Liu, Y.X.Peng, X.Q.Ge, L.Y.Shi, W. Huang, Dalton Trans., 2015, **44**, 237-246.
- [8] L.N. Sun, X.Q.Ge, J. L.Liu, Y.N.Qiu, Z.W.Weil, B.Tian, L.Y.Shi, Nanoscale, 2014, **6**, 13242-13252
- [9] M.Miao, J.P.Zhao, X.Feng, Y.Cao, S.M.Cao, Y.F.Zhao, X.Q.Ge, L.N.Sun, L.Y.Shi, J.H.Fang, J. Mater. Chem. C, 2015, **3**, 2511-2517.
- [10] X. Z.Fan, X. Liu. Optical instruments, 2002, **3**, 38-43.
- [11] G. Vicentini, L.B. Zinner, J. Zukerman-Schpector, K. Zinner, Coord. Chem. Rev., 2000, **196**, 353-382.

- [12] Z.Z. Yan, Y. Tang, W.S. Liu, H.X. Cui, M.Y. Tan, *J. Fluoresc.*, 2008,**18**, 473-478.
- [13] J. Dhanaraj, R. Jagannathan, T.R.N. Kutty, L. Chung-Hsin, *J. Phys. Chem. B*, 2001,**105**, 11098-11105.
- [14] J.Y. Chane-Ching, G. Martinet, P.J. Panteix, C. Brochard, A. Barnabe, M. Airiau, *Chem. Mater.*, 2011,**23**, 1070-1077.
- [15] K. Driesen, R. Van Deun, C. Gorller-Walrand, K. Binnemans, *Chem. Mater.*, 2004,**16**, 1531-1535.
- [16] P. Lenaerts, K. Driesen, R. Van Deun, K. Binnemans, *Chem. Mater.*, 2005,**17**, 2148-2154.
- [17] F.L.Xu, Y.Xu, D.G.Yu, J. University of Shanghai for Science and Technology., 2015, 37,165-168.
- [18] R. Van Deun, D. Moors, K. Binnemans, *J. Mater. Chem.*, 2003, **13**, 1520-1522.
- [19] Y. Li, B. Yan, *J. Phys. Chem. C*, 2008,**112**, 3959-3968.
- [20] Y.Li, W.Qian, X. Wang, W.T. Sha, Y.W. Zhang, W.K. Jiang, *Photochem. Photobio.*, 2011,**87**,618-625.
- [21] Y.Li, J.L.Wang, W.Chain, X.Wang, Z.Jin, X.Q.Li, *RSC Adv.*,2013,**3**,14057-14065
- [22] Y.J. Gu, B. Yan, Y.Y. Li, *J. Solid State Chem.*, 2012, **190**, 36-44.
- [23] Y.J.Li,B.Yan,Y.Li, *J. Solid State Chem.*, 2010, **183**, 871-877.
- [24] Y.J.Li,B.Yan,Y.Li, *Chem. Asian J.* 2010, **5**, 1642-1651.
- [25] P. Lenaerts, A. Storms, J. Mullens, J. Dhaen, C. Gorller-Walrand, K. Binnemans, K. Driesen, *Chem. Mater.*, 2005,**17**,5194-5201.
- [26] J.W. Wei, J. J. Shi, H. Pan, Q.F. Su, J.B. Zhu, Y. Shi, *Microp. Mesop. Mater.*, 2009, **117**,596-602.
- [27] M.C. Goncalves, V.D. Bermudez, R.A. Sa Ferreira, L.D. Carlos, D. Ostrovskii, J. Rocha, *Chem. Mater.*, 2004, **16**, 2530-2543.
- [28] P.A Tanner, B. Yan, H.J. Zhang, *J. Mater. Sci.*, 2000,**35**, 4325-4328.
- [29] P.C.R. Soares-Santos, H.I.S. Nogueira, V. Felix, M.G.B. Drew, R.A.S. Ferreira, L.D. Carlos, T. Trindade, *Chem. Mater.*, 2003, **15**, 100-108.
- [30] B. Yan, H.F. Lu, *Inorg. Chem.*, 2008, **47**, 5601-5611.
- [31] Y.J. Gu, B. Yan, X.F. Qiao, *J. Solid State Chem.*, 2013,**199**, 116-122.
- [32] A. Mech, A. Monguzzi, F. Cucinotta, *Phys. Chem. Chem. Phys.*, 2011, **13**, 5605-5609.
- [33] B. Yan, Y.Y. Li, X.F. Qiao, *Microp. Mesop. Mater.*, 2012, **158**,129-136.

- [34] F. Eckes, V. Bulach, A. Guenet, C.A. Strassert, L. De Cola, M.W. Hosseini, *Chem. Commun.*, 2010, **46**,619-621.
- [35] Y. Li, B. Yan, *Solid State Sci.*, 2009, **11**, 994-1000.
- [36] L.N. Sun, H.J. Zhang, C.Y. Peng, J.B. Yu, Q.G. Meng, L.S. Fu, F.Y. Liu, X.M. Guo, *J. Phys. Chem. B*, 2006,**110**, 7249-7258.
- [37] E.S. Teotonio, J.G.P. Espinola, H.F. Brito, O.L. Malta, S.F. Oliveria, D.L.A. De Foria, C.M.S. Izumi, *Polyhedron*, 2002,**21**, 1837-1844.
- [38] Y.S. Liu, W.Q. Luo, R.F. Li, G.K. Liu, M.R. Antonio, X.Y. Chen, *J. Phys. Chem. C*, 2008,**112**, 686-694.
- [39] J.C. Boyer, F. Vetrone, J.A. Capobianco, A. Speghini, M. Bettinelli, *J. Phys. Chem. B*, 2004, **108**, 20137-20143.

TOC



Novel polymeric mesoporous luminescent hybrids have been synthesized by linking the binary and ternary Ln^{3+} complexes to polyacrylamide-functionalized mesoporous SBA-16 in situ. As a result, all the hybrids exhibit high surface area, uniform mesostructure, efficient intramolecular energy transfer and higher luminescence intensity. The excellent luminescent properties of these materials, together with the highly ordered mesoporous structure will expand their applications in optical or electronic areas.